PCCP

PAPER

View Article Online
View Journal | View Issue

Cite this: *Phys. Chem. Chem. Phys.*, 2021, **23**, 6190

Transition anionic complex in trihexyl(tetradecyl)-phosphonium-bis(oxalato)borate ionic liquid – revisited†

Manishkumar R. Shimpi, *[a] Patrick Rohlmann, [b] Faiz Ullah Shah, [a] Sergei Glavatskih [bcd] and Oleg N. Antzutkin *[ae]

It was found that Li[BOB]·nH$_2$O salts were not readily suitable for the synthesis of high-purity orthoborate-based tetraalkylphosphonium ionic liquids, as exemplified here for trihexyl(tetradecyl)phosphonium bis-(oxalato)borate, [P$_{6,6,6,14}$][BOB]; along with [BOB]$^-$, a metastable transition anionic complex (TAC) of dihydroxy-(oxalato)borate with oxalic acid, [B(C$_2$O$_4$)(OH)$_2$·(HOOC–COOH)]$^-$, was also formed and passed into the ionic liquid in the course of the metathesis reaction with trihexyl(tetradecyl)phosphonium chloride. On the contrary, Na[BOB] was found to be a more suitable reagent for the synthesis of this IL, because [BOB]$^-$ anions safely passed into the final IL without hydrolysis, when metathesis reactions were performed using aqueous-free media. Since ultra-pure Na[BOB] is not commercially available, in this work, a preparation protocol for ultra-pure (>99%) Na[BOB] was developed: (i) molar ratios of boric and oxalic acids were optimised to minimise boron-containing impurities, (ii) the Na[BOB] product was thoroughly purified by sequential washing of a fine powder product in hot acetonitrile and ethanol and (iii) characterised using powder X-ray diffraction and solid-state ^{11}B MAS NMR spectroscopy. The physico-chemical properties of the prepared boron-impurity-free IL, *i.e.*, its density, viscosity, electric conductivity, glass-transition temperature and thermal stability, were found to be significantly different from those of the previously reported [P$_{6,6,6,14}$][BOB], containing *ca.* 45 mol% of TAC, [B(C$_2$O$_4$)(OH)$_2$·(HOOC–COOH)]$^-$. It was found that a high-purity [P$_{6,6,6,14}$][BOB] prepared in this work has a considerably lower viscosity, a higher viscosity index and a wider electro-chemical window (ECW) compared to those of the sample of [P$_{6,6,6,14}$][BOB] with *ca.* 45 mol% of TAC. Interestingly, [B(C$_2$O$_4$)(OH)$_2$·(HOOC–COOH)]$^-$ in the latter sample almost completely transformed into [BOB]$^-$ anions upon heating of the IL sample at 413 K for 1 hour, as confirmed using both ^{11}B and ^{13}C NMR. Therefore, in this work, apart from a well-optimised synthetic protocol for boron-impurity-free [P$_{6,6,6,14}$][BOB], implications of boron-containing transition anionic complexes in tetraalkylphosphonium-orthoborate ILs used in different applications were highlighted.

Received 9th November 2020,
Accepted 3rd February 2021

DOI: 10.1039/d0cp05845a

rsc.li/pccp

Introduction

Ionic liquids (ILs) belong to a special class of ionic materials, which are liquids below 373 K, that have negligible vapour pressure, a wide temperature range of stability, and high electric conductivity and can be functionalised for task-specific applications.[1] However, impurities present in ILs are often overlooked and do not receive appropriate attention. Some impurities in ILs can be difficult to detect and identify. Widely explored hydrophobic ILs with low viscosity at near room temperatures, such as ILs with the fluorine-containing anion [(CF$_3$SO$_2$)$_2$N]$^-$ ([Tf$_2$N]$^-$), were found to be considerably more cytotoxic compared to the ILs with their chloride (Cl$^-$) analogues, as revealed by IL-induced apoptosis in HeLa cells.[2,3] Therefore, ILs with desired properties (low viscosity, high ionic conductivity, wide electro-chemical window, *etc.*) but with "greener" anions are still urgently needed. Many different classes of ILs have been investigated in laboratory studies and various industrially relevant applications, such as in fuel and solar cells, as catalysts, in pharmaceuticals, for biomass treatment, for gas storage, as electrolytes, as solvents for catalytic reactions[1,4–6] and in lubrication.[7–16] Plenty of on-going research

[a] *Chemistry of Interfaces, Luleå University of Technology, SE-97 187, Luleå, Sweden. E-mail: Manishkumar.Shimpi@ltu.se, Oleg.Antzutkin@ltu.se*
[b] *System and Component Design, KTH Royal Institute of Technology, SE-10 044 Stockholm, Sweden*
[c] *School of Chemistry, University of New South Wales, UNSW Sydney NSW 2052, Australia*
[d] *Department of Electromechanical, Systems and Metal Engineering, Ghent University, B-9052 Ghent, Belgium*
[e] *Department of Physics, Warwick University, CV4 7AL, Covertly, UK*

† Electronic supplementary information (ESI) available. See DOI: 10.1039/d0cp05845a

studies focus on utilising novel ILs in various emerging applications: artificial photosynthesis,[17] hypergolic propellants,[18] phenol-based hybrid ILs for ionic conductors,[19] oligomeric ILs for exfoliation of graphite with high yield and selectivity towards single-layer graphene,[20] crystal engineering using IL as the solvent to design unique crystallisation environment[21] and even as lubricants for demanding space applications.[14] ILs are attractive for tribological applications due to their properties, which conventional lubricants do not have.[7–16]

It has been pointed out by many researchers in the field of ionic liquids that residual impurities do significantly alter the properties of ILs. In particular, viscosity of ILs is strongly dependent on the fractions of percent amounts of residual solvents and water, in addition to halides as a result of either misbalanced metathesis reactions or the propensity of targeted anions to be washed out from the final product together with cations of alkali metals (Li^+ or Na^+). However, the synthesis of high purity (>99 wt%) ILs is a challenging task, because, they, as universal solvents, are prone to hold impurities as solutes. The task of quantifying and controlling of impurities in ILs, such as the byproducts of alkylation reactions, unreacted or half-reacted reagents, traces of organic solvents, halides, metal ions, water, *etc.*, is a ''must'', since impurities may severely affect the physico-chemical properties of ILs, such as their density, viscosity, conductivity, glass-transition temperature, thermal stability, *etc.* and, therefore, their performance in different applications. Water and traces of solvents used during the IL preparation are among the most abundant impurities irrespective of whether ILs are hydrophilic or hydrophobic. It has been reported that the viscosity of $[C_2C_1Im][Tf_2N]$, $[C_4C_1Im][Tf_2N]$ and $[C_4C_1Im][PF_6]$, which are hydrophobic ILs, is strongly affected if traces of water are present in these ILs.[22] Andanson *et al.* have thoroughly measured and quantified the effect of water as a solute on both density and viscosity of a number of imidazolium-based ILs.[23] The electric conductivity of imidazolium-based ILs is also dependent on the water content of these systems.[24,25] On the other hand, halide based impurities in ILs may lead to dealkylation reactions of alkylimidazolium, tetraalkylphosphonium, tetraalkylammonium and other types of cations, in particular at elevated temperatures, which may, in turn, also affect the electrochemical stability window (ECW) and other properties of ILs.[26] Hence, there is a need for a more thorough quantification of halide impurities in ILs, either using total reflection X-ray fluorescence spectrometry[27] or using the more widely used ESI-MS or/and ICP-MS.[28] Traces of halides (Cl^-, Br^- or I^-) and halogen containing solvents can pass to ILs from imidazolium and phosphonium (or other) halides used as the reagents in the metathesis reaction step, followed by the extraction of the final product usually using dichloromethane or chloroform.[9]

Another important aspect in the research field of ILs is the fact that due to the improper characterisation of impurities present in ILs (for example, in $[C_4C_1Im][PF_6]$), the melting point and viscosity may differ significantly in different reports.[22,29–31] Such uncertain data are a barrier for the use of ILs in research and in industrial applications. Therefore, the ability to control impurities (unreacted reactants, residual solvents, traces of water, halides or degraded intermediate ions, by-products, *etc.*) is crucial to achieve reproducible results and targeted properties of ILs. Specifically, for orthoborate-based ILs there are challenges in removing the boron-containing impurities from the ILs, *i.e.* the by-products in the synthesis of orthoborate anions and products of their decomposition in the course of the metathesis reaction. Since boron is considered to be a tribologically active element, these boron-containing impurities, when present in percent and fractions of percent amounts in ILs, may have serious implications in tribological applications, in which ILs are used as neat lubricants.

In the original work of Angell and co-workers back in 2003, synthetic protocols have been developed for the first orthoborate-based ILs, including those with bis(oxalato)borate anions having a wide ECW, with a specific target for electrochemical applications.[32] In their protocols, both lithium and sodium salts of orthoborate anions as reagents in the metathesis reactions have been used.[32] Though data on the identity and yields of the prepared ILs have been reported, no details on purity of the synthesised ILs have been given, apart from the fact that, when ILs are prepared using Li[BOB] salts, small ^{7}Li NMR signals are detected. The latter was attributed to the traces of residual lithium ions in the ILs.[32] Later Li[BOB][33–36] and Na[BOB],[37,38] have been tested as components for new types of electrolytes in lithium and sodium ion batteries and considered as possible alternatives for the currently used $Li[PF_6]$ and $Na[PF_6]$ prone to give rise to toxic HF(*g*) and POF_3(*g*) in case of battery fire accidents.[39] It is also worth considering that Li[BOB] crystallises in the form of solvates from solvents like water ($Li[BOB]\cdot nH_2O$), acetonitrile, acetone, dimethoxylethane and 1,3-dioxane, among others.[33] Though ultra-high purity (99.99%) Li[BOB] is commercially available, the solvate molecules may hydrolyse $[BOB]^-$ anions in the course of metathesis reactions and give rise to oxalic acid and other borate based anions, which may then pass into the final product (ionic liquid) as ionic impurities or as transition anionic complexes. Recently, Schmitz *et al.* have reported on the synthesis of high-purity imidazolium tetrafluoroborate and bis(oxalato)borate ILs, again targeting the electro-chemical applications of these ILs.[40] Surprisingly, special precautions about the additional purification of neither the reagents (starting purity of 97–98%) and reaction intermediates, nor the final products (ILs) have been given in the suggested synthetic protocol.[40] Though ion chromatography and Karl Fisher titration data suggested a 99.9% purity of the synthesised ILs and the ^{1}H and ^{13}C NMR spectra of the ILs dissolved in DMSO-d_6 did not show significant levels of impurities, ^{11}B (and ^{7}Li) NMR spectra that usually clearly reveal boron (and lithium) impurities have not been reported.[40] It is highly recommended to obtain ^{11}B and ^{7}Li (and ^{13}C, ^{31}P, ^{23}Na and ^{15}N, when relevant) NMR spectra of neat ILs since some of the impurities may precipitate out from the NMR-solvent/IL solution during sample preparation and, thus, can be overlooked. It is also noteworthy that tetraalkylphosphonium orthoborate ILs have not been synthesised and characterised in the two aforementioned reports on [BOB]-based ILs.[32,40]

In this work, viscosity of trihexyl(tetradecyl)phosphonium bis(oxalato)borate, $[P_{6,6,6,14}][BOB]$, synthesised using Na[BOB]

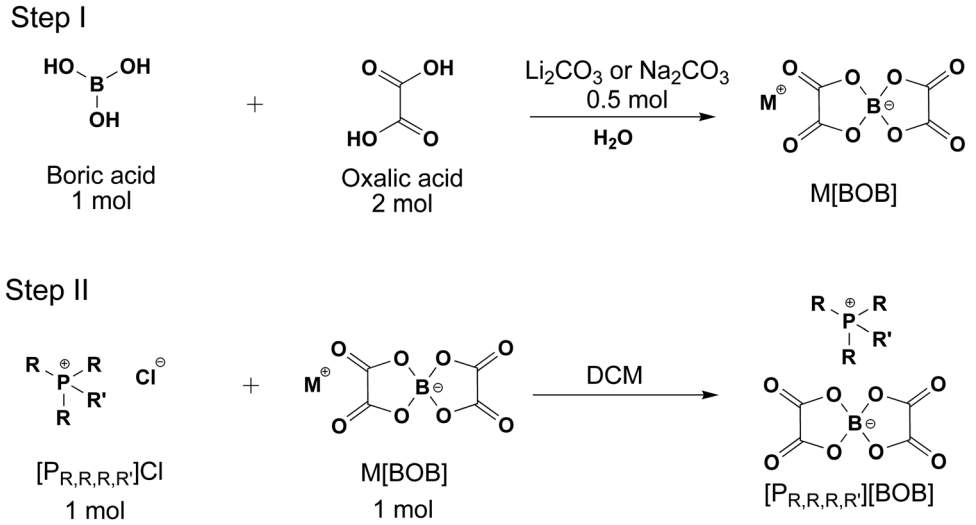

Scheme 1 Synthesis of tetraalkylphosphonium bis(oxalato)borate ILs, where R and R′ are alkyl (C_nH_{2n+1}) groups with n = 6 and 14, respectively, and M^+ denotes either Li^+ or Na^+.

instead of Li[BOB]·nH$_2$O, as in one of our previous publications (a sample that is denoted here as [P$_{6,6,6,14}$][BOB]^9), was found to be significantly lower than the values reported previously.[9] For tetraalkylphosphonium orthoborate-based ILs, a two-step synthesis using lithium carbonate has been adapted from ref. 9, and we here followed a similar synthetic protocol using Na_2CO_3 instead of Li_2CO_3 and with a significantly larger excess of oxalic acid over boric acid to shift the reaction equilibrium towards Na[BOB] obtained in Step I (see Scheme 1). It was also found that, apart from a dramatic difference in viscosity, the previously prepared sample of [P$_{6,6,6,14}$][BOB]^9 contained *ca.* 2 wt% of "strongly trapped" water even after extensive (a few weeks) vacuum drying at 333 K, while [P$_{6,6,6,14}$][BOB] prepared in this work contained only 0.06 wt% of water. A thorough ^{11}B, ^{1}H and ^{13}C NMR analysis further supported by mass spectrometry and TGA, have revealed that in the synthesis involving lithium carbonate a transition anionic complex (TAC) of dihydroxy(oxalato)borate with oxalic acid, $[B(C_2O_4)(OH)_2\cdot(HOOC–COOH)]^-$, was also formed and passed into the ionic liquid together with $[BOB]^-$ in the course of the metathesis reaction in Step II (see Scheme 1). The presence of TAC in the sample [P$_{6,6,6,14}$][BOB]^9 caused a large increase in viscosity and significant changes in other properties of the IL, presumably due to hydrogen bonds stabilising the internal structure of the TAC and the aggregates of TAC with $[BOB]^-$ anions. Interestingly, the majority of the TAC trapped in the IL matrix have transformed into $[BOB]^-$ upon heating of the sample [P$_{6,6,6,14}$][BOB]^9 at 413 K for an hour. The latter approach was implemented after useful information was obtained from tribotests performed at steel–steel contacts lubricated using either [P$_{6,6,6,14}$][BOB] or [P$_{6,6,6,14}$][BOB]^9: while the coefficients of friction were significantly different at 353 K, the friction performance became almost the same for these two samples at 413 K.[41]

In this work, we also report on the step-by-step synthesis and characterisation of [P$_{6,6,6,14}$][BOB] with a thoroughly controlled high purity, using a range of spectroscopic and analytical methods. Our objective was to prepare ILs with minimum traces of boron based impurities (including TACs) and with lowest possible levels of residual water and halides and then to tabulate the physico-chemical properties of the prepared ILs. We made the following precautions and modifications in the synthetic protocol in order to achieve these objectives: (i) we used aqueous media synthesis (the "greenest" solvent) instead of tetrahydrofurane as in some other works, main reagents (boric and oxalic acids) of ultra-high purity (99.999%), supporting reagents (sodium/lithium carbonate) of high purity (99.9%) in synthetic Step I and commercial trihexyl(tetradecyl)-phosphonium chloride of the highest available purity (>98%) in Step II. (ii) We have found that Na[BOB] is more suitable compared to Li[BOB] for the preparation of high-purity [P$_{6,6,6,14}$][BOB]: Li[BOB] in our preparation was always a mixture of anhydrous Li[BOB] and Li[BOB]·nH$_2$O. In addition, Li[BOB] undesirably converted into lithium oxalate monohydrate in the presence of water. (iii) We used a significant excess of oxalic acid (3 : 1 molar ratio of oxalic acid : boric acid instead of 2 : 1 as required for the reaction) to shift the reaction equilibrium towards the desired intermediate product Na[BOB]. (iv) We have further purified Na[BOB] by washing the fine powder from Step I with hot acetonitrile and ethanol in order to remove TAC and other boron-based impurities. (v) In addition to liquid state ^{1}H, ^{11}B, ^{13}C, ^{31}P, NMR, PXRD, ICP-MS and Karl Fischer titration, solid-state ^{11}B MAS NMR was used as a tool for tracing the boron containing impurities in solid Na[BOB] prepared in Step I, while liquid state ^{11}B NMR in boron-free zirconia rotors was employed to confirm the high purity of the prepared liquid [P$_{6,6,6,14}$][BOB]. Viscosity, density, thermal stability, electric conductivity and the electrochemical stability window (ECW) of [P$_{6,6,6,14}$][BOB] were compared with previously reported data for the sample of [P$_{6,6,6,14}$][BOB]^9 containing *ca.* 45 mol% of TAC as estimated using ^{11}B NMR.

Results and discussion

Step I: synthesis of Na[BOB]

In the course of preparing a lithium salt of bis(oxalato)borate in aqueous media (see Scheme 1, Step I), a mixture of anhydrous Li[BOB] and lithium bis(oxalato)borate monohydrate, Li[BOB]·H_2O, was obtained (see Fig. S1 in the ESI†). It is known that anhydrous Li[BOB] is hygroscopic and it may slowly hydrolyse resulting in $B(C_2O_4)(OH)$ and $LiB(C_2O_4)(OH)_2$ compounds, when exposed to humid air.[42] In contrast, a sodium salt of bis(oxalato)borate, Na[BOB], though synthesised in a similar way, was found to be moisture stable. Powder X-ray diffraction (PXRD) was found to be a very useful technique to identify Li[BOB], Li[BOB]·H_2O and Na[BOB] as well as crystalline impurities, as confirmed by comparing with the simulated powder X-ray diffraction patterns of the known single-crystal structures (Fig. 1). This technique is fast, versatile, non-destructive and the results are relatively easy to interpret for crystalline materials. The PXRD pattern of a crude sample of Na[BOB] revealed the presence of small amounts of crystalline impurities. Following a purification method of Lall-Ramnarine *et al.* developed for Na[BOB],[43] this sample was additionally washed using hot acetonitrile to remove impurities (highlighted using red boxes and arrows in Fig. 1) from Na[BOB]. Moreover, the crystallinity of the Na[BOB] material after washing with hot acetonitrile was enhanced (indicated by an increase in the intensity of reflections, indicated using a double-headed arrow in Fig. 1). However, amorphous impurities in the solid bulk material are not detected using this technique and, therefore, can be overlooked if PXRD is used as the only analytical tool. In addition, we have collected PXRD of Na[BOB] exposed to air at different time intervals (data not shown). In contrast to Li[BOB], which is sensitive to humidity, there is no noticeable change in the PXRD patterns of Na[BOB] exposed to humid air over time.

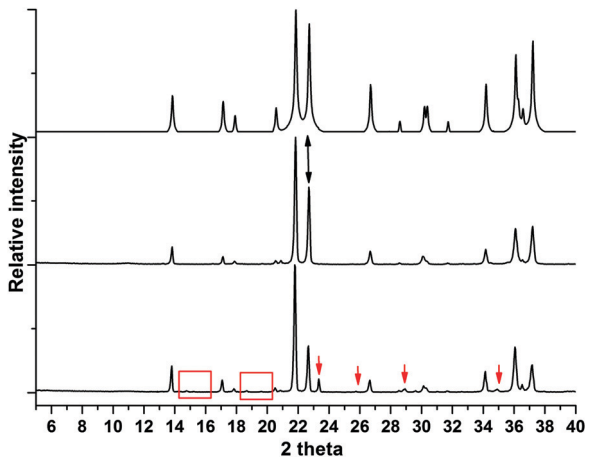

Fig. 1 Powder XRD patterns of a crude sample of Na[BOB] obtained in Step I of Scheme 1 (bottom), purified Na[BOB] by washing of the crude sample in hot acetonitrile (middle), and a simulated PXRD pattern generated from the known single-crystal structure of Na[BOB] (top). Red boxes and arrows indicate impurities present in the crude material before purification. The double-headed arrow shows an increase in the intensity of reflections and, thus, in crystallinity of the material after washing and recrystallisation in hot acetonitrile.

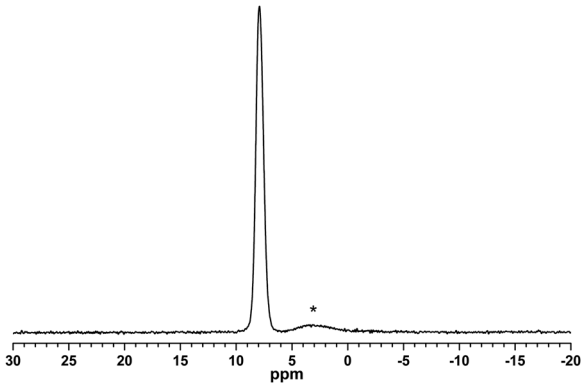

Fig. 2 A single-pulse ^{11}B MAS NMR spectrum of a Na[BOB] powder sample after washing of the crude material with hot acetonitrile. The asterisk at *ca.* 3 ppm denotes a residual boron-containing impurity assigned to the reaction intermediate anionic species $[B(C_2O_4)(OH)_2{\cdot}H_2C_2O_4]^-$.

A solid-state ^{11}B MAS NMR spectrum of the Na[BOB] powder after washing of the crude material with hot acetonitrile is shown in Fig. 2. In addition to a major resonance line at 7.8 ppm assigned to the boron sites in solid Na[BOB], there is a minor broader resonance line around 3 ppm, which corresponds to the boron sites in boron-containing impurities, most probably a reaction intermediate species, *i.e.*, a "1 : 1" product of the reaction of boric acid with oxalic acid, $[B(C_2O_4)(OH)_2]^-$, as suggested in previous reports.[42,44] Therefore, in contrast to PXRD, which cannot detect the amorphous part of the same sample, single-pulse solid-state ^{11}B MAS NMR reveals signals from the whole bulk sample, *i.e.* from both polycrystalline and amorphous parts of the boron-containing material. Because of the negative charge of the preliminary assigned reaction intermediate (see Fig. 2), it can also pass together with tetraalkylphosphonium cations (and $[BOB]^-$ anions) into the final product $[P_{6,6,6,14}][BOB]$ during the metathesis reaction (Step II in Scheme 1). Therefore, the crude material of Na[BOB] washed with hot acetonitrile was further purified by washing in ice-cold ethanol as suggested by Lall-Ramnarine *et al.*[43] Solid-state ^{11}B MAS NMR spectra of the treated solid material revealed a further minor reduction in the level of boron-containing impurities having a ^{11}B chemical shift at *ca.* 3 ppm (see Fig. S2 in the ESI†), while no significant changes in the PXRD patterns of the samples after additional washing with ice-cold ethanol were noticed, as expected if the impurities were amorphous in nature.

To further explore the working hypothesis that an intermediate of the reaction of boric acid with oxalic acid (Step I in Scheme 1) is a species containing another orthoborate anion, $[B(C_2O_4)(OH)_2]^-$, reaction mixtures with different ratios of boric acid to oxalic acid (and one-half mole of sodium carbonate) were tested. Single-pulse ^{11}B MAS NMR spectra of the prepared powder materials using the following molar ratios of the reactants ($H_3BO_3 : H_2C_2O_4 : Na_2CO_3$) = (1.0 : 1.0 : 0.5); (1.0 : 1.5 : 0.5); (1.0 : 2.0 : 0.5); (1.0 : 2.1 : 0.5); (1.0 : 2.5 : 0.5) and (1.0 : 3.0 : 0.5) are shown in Fig. 3. Three main resonance lines corresponding to three different types of boron sites in the

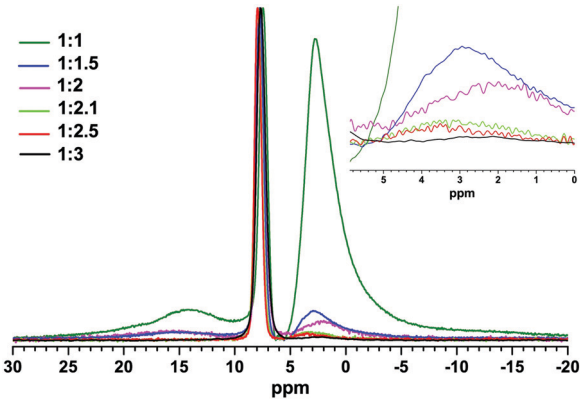

Fig. 3 Single-pulse ^{11}B MAS NMR spectra of powder samples obtained in the synthetic Step I (see Scheme 1) with different molar ratios of boric acid to oxalic acid (the inset on the left depicts the molar ratios of (H_3BO_3 : $H_2C_2O_4$)). The inset on the right shows a decrease in intensity of the resonance line corresponding to boron-based reaction intermediates following an increase in the relative amounts of oxalic acid to boric acid.

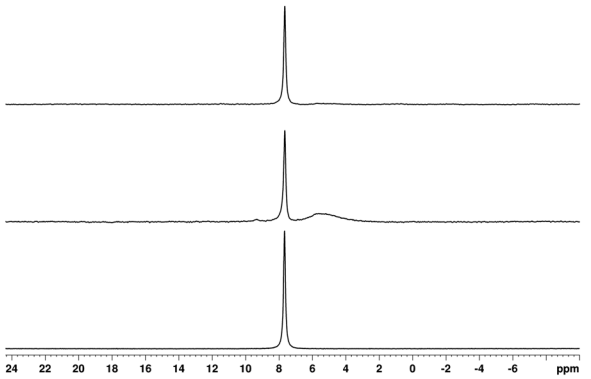

Fig. 4 Solution ^{11}B NMR (in $CDCl_3$) spectra of [$P_{6,6,6,14}$][BOB] (bottom), [$P_{6,6,6,14}$][BOB][9] (middle), and [$P_{6,6,6,14}$][BOB][9] after heating of the sample at 413 K for 1 hour (top).

final materials, with different integral intensities depending on the molar ratios of the reactants, were detected: a narrow resonance line at *ca.* 7.8 ppm with a linewidth (at the half height) of *ca.* 1 ppm assigned to the boron sites of the solid Na[BOB] salt was flanked with two broad resonance lines, one of which between 25 and 10 ppm reveals the presence of three-coordinate boron containing impurities, such as unreacted boric acid and borates,[45] while the third resonance line, between *ca.* +5 and −5 ppm, could be assigned to species containing tetrahedrally coordinated boron, including sodium dihydroxy(oxalato)borate, $[B(C_2O_4)(OH)_2]^-$, as one of the main intermediates in Step I of the reaction as discussed above.

For all the reaction mixtures, apart from the expected product, Na[BOB], solid-state ^{11}B NMR clearly reveals the presence of other boron-containing compounds, both reactants (boric acid) and reaction intermediates, the integral intensities of which, however, were gradually decreased with an increase in the molar ratios of oxalic acid to boric acid under, otherwise, similar reaction conditions. Moreover, the deconvolution of ^{11}B NMR data (see Table 1) indicates that >99.2 mol% pure Na[BOB] could be prepared using a 50% molar excess of oxalic acid, *i.e.* at the (1.0 : 3.0) molar ratio of boric acid to oxalic acid, as previously suggested by Carr *et al.*[44] Therefore, it can be concluded that a significant excess of oxalic acid over boric acid was required to convert boron containing intermediates to the desired Na[BOB]. Such an excess of oxalic acid was required to maintain the reaction conditions at lower pH to reach a fully protonated state of oxalic acid and, thus, to limit the electrostatic repulsion between the reactants, *i.e.* negatively charged tetrahydroxoborate and oxalate anions.[44] Therefore, the reaction equilibrium would then shift towards the desired product, bis(oxalato)borate anions.[44,46] Note that an excess of oxalic acid present in the crude product material can then be easily washed out using hot acetonitrile and cold ethanol as previously reported by Lall-Ramnarine *et al.*[43]

Table 1 Relative integral intensities for two main boron sites (in mol%) obtained by the deconvolution of ^{11}B MAS NMR spectra of samples prepared with different molar ratios of boric acid and oxalic acid

Molar ratios of (boric acid : oxalic acid)	Na[BOB] (δ(^{11}B) = 7.8 ppm, integrated interval [9; 7] ppm) mol%	Impurities (the TAC, integrated interval [5; −5] ppm) mol%
1.0 : 1.0	17.2	69.9
1.0 : 1.5	64.0	22.0
1.0 : 2.0	69.4	17.1
1.0 : 2.1	92.8	7.2
1.0 : 2.5	94.6	5.4
1.0 : 3.0	99.2	0.8

The ionic liquid [$P_{6,6,6,14}$][BOB] was then prepared in the metathesis reaction (Step II in Scheme 1), in which a thoroughly purified Na[BOB] obtained in the synthesis using the (1.0 : 3.0) molar ratio of boric acid to oxalic acid, and trihexyl(tetradecyl)phosphonium chloride were mixed together in equimolar amounts in dichloromethane with the following liquid–liquid phase separation and washed using double-distilled water (see the Experimental section for more details). A solution ^{11}B NMR spectrum of [$P_{6,6,6,14}$][BOB] in $CDCl_3$ displays a single resonance line at 7.67 ppm (Fig. 4 bottom) that confirms the individual character of the anionic part of this IL and low levels of boron containing impurities that was invisible with NMR in this sample. In contrast, a sample of [$P_{6,6,6,14}$][BOB][9] previously prepared by us using lithium carbonate shows a boron containing impurity (see a broad resonance line in the range from 3 to 6 ppm in Fig. 4 middle). Integration of these two resonances has revealed that these impurities are present in [$P_{6,6,6,14}$][BOB][9] at amounts corresponding to *ca.* 45 mol% of boron (see Fig. S19 in the ESI†).

Solution ^{13}C NMR has assisted us to reveal the nature of the boron-containing impurities in [$P_{6,6,6,14}$][BOB][9], while the carbonyl carbon sites in [BOB] anions have a chemical shift δ(^{11}B) = 158.91 ppm (Fig. 5 bottom, [$P_{6,6,6,14}$][BOB]),[43] a sample of [$P_{6,6,6,14}$][BOB][9] does contain carbonyl and/or carboxyl groups, which are more deshielded, *i.e.* at δ(^{13}C) = 161.83 and 163.08 ppm (Fig. 5 middle). The latter chemical shift is very close to that of the carboxyl groups of oxalic acid or a singly deprotonated oxalate anion, while δ(^{13}C) = 161.83 ppm could correspond to the carbonyl carbons in the oxalate ligand of the dihydroxy(oxalato)borate

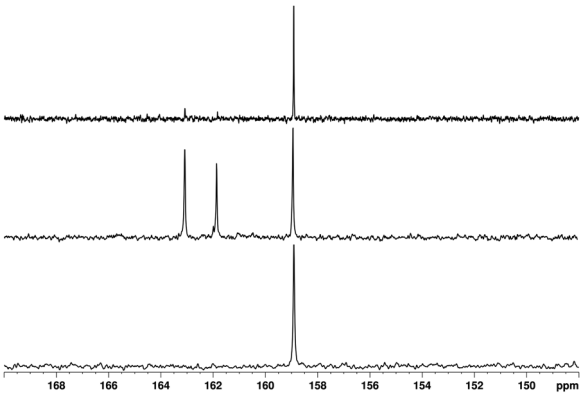

Fig. 5 Solution ^{13}C NMR (in $CDCl_3$) spectra of $[P_{6,6,6,14}][BOB]$ (bottom), $[P_{6,6,6,14}][BOB]^9$ before the heat treatment (middle), and $[P_{6,6,6,14}][BOB]^{9-}$ after the heat treatment of the sample at 413 K for 1 hour (top). A 30°-excitation pulse with the recycling delay of 30 s was used to minimise the NMR signal saturation of the carbon sites in the $[BOB]^-$ (158.91 ppm) and the TAC (161.83 and 163.08 ppm) anions. From 1024 (bottom and middle spectra) to 1512 (top spectrum) signal transients were accumulated for achieving of a reasonably good signal-to-noise ratio (S/N > 10). The whole range ^{13}C NMR spectra with different experimental parameters are also given in the ESI (Fig. S9, S10, S15 and S16).†

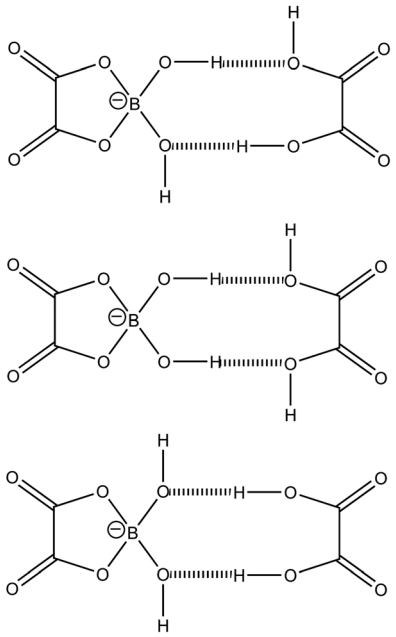

Fig. 6 Possible structures of TAC: $[B(C_2O_4)(OH)_2{\cdot}(HOOC–COOH)]^-$.

anion, which is also detected using ^{11}B NMR as a broad resonance line at *ca.* 5.5 ppm. Both oxalate anions and dihydroxy(oxalato)borate anions are ionic and, therefore, could easily pass into the final sample of the IL in the second reaction step (the metathesis reaction, Scheme 1).

Interestingly, upon heating a sample of $[P_{6,6,6,14}][BOB]^9$ at 413 K for 60 minutes, a broad resonance line at *ca.* 5.5 ppm in the ^{11}B NMR spectrum disappeared (see Fig. 4 top). In addition, the resonance lines at $\delta(^{13}C)$ = 161.83 and 163.08 ppm have also almost (but not completely) disappeared from the ^{13}C NMR spectrum. These two facts in combination do suggest the presence of a TAC with 1 : 1 molar composition of the dihydroxy(oxalato)borate anion with oxalic acid, *i.e.* $[B(C_2O_4)(OH)_2{\cdot}(HOOC–COOH)]^-$ in the IL sample $[P_{6,6,6,14}][BOB]^9$. We have also performed ESI-MS on these two samples (see Fig. S21 and S23 for the negative-ion modes, ESI†). However, though ESI-MS of $[P_{6,6,6,14}][BOB]^9$ does suggest the presence of anionic moieties corresponding to TAC and its dehydration products (such as $B(C_2O_4)O^-$ with *ca.* 114 a.u., which is $B(C_2O_4)(OH)_2$ minus H_2O), this method is not quantitative. Moreover, neutral molecules, which may form during the *in situ* decomposition of TAC (such as fully protonated oxalic acid) are not detectable by ESI-MS.

Fig. 6 illustrates three possible configurations of the suggested TAC, in which geometries of the OH groups are hypothesised based on the X-ray single crystal structures of different borates.[47] At elevated temperatures, TAC is transformed into $[BOB]^-$ releasing two water molecules into the matrix of the IL sample. Note that this reaction with the formation of covalent chemical bonds between the oxalate ligand and boron is probably irreversible. This is because water molecules will be gradually expelled by the hydrophobic aliphatic chains of $[P_{6,6,6,14}]^+$ cations from regions, in which the original TACs were aggregated together and held by hydrogen bonding networks. These types of interactions lead to dramatic changes in properties of the IL, such as density, viscosity, conductivity, and thermal stability, as will be discussed below.

The elemental analysis and water content

Sodium and chlorine content was determined using ICP-MS elemental analysis, which revealed 2 ppm of sodium and 50 ppm of chlorine in $[P_{6,6,6,14}][BOB]$, thus, confirming that the metathesis reaction was well-balanced and complete and the chlorine containing solvent (dichlorometane) was almost completely removed from the sample by long-term degassing in a vacuum oven at elevated temperatures (ranging from 313 to 323 K).

Water is arguably one of the most important impurities of ILs that needs to be considered, because water may significantly affect the physicochemical properties and performance of ILs (*e.g.* their thermal stability, glass transition temperature, viscosity, density, and electric conductivity). It is noteworthy that even in hydrophobic ILs traces of water may be trapped near the polar groups of ions after the metathesis reaction and washing of the final product. The indirect Karl Fischer method was used to determine the water content in $[P_{6,6,6,14}][BOB]$ and $[P_{6,6,6,14}][BOB]^9$ before the heat treatment: Water content was found to be 0.06 and 1.2 wt% in these samples, respectively. Water content previously measured in $[P_{6,6,6,14}][BOB]^9$ using the direct Karl Fischer method was 2.323 and 2.026 wt% before and after drying at 333 K for 48 h.[9] Note that data obtained using the indirect Karl Fischer method are more reliable, because methanol, used as one of reagents in the direct Karl Fischer titration, causes the hydrolysis of $[BOB]^-$ anions and, thus, leads to overestimated amounts of water present in all [BOB]-based ILs.

Thermal stability

Thermogravimetric analysis (TGA), in both the dynamic and isothermal modes, was used to study the thermal stability and

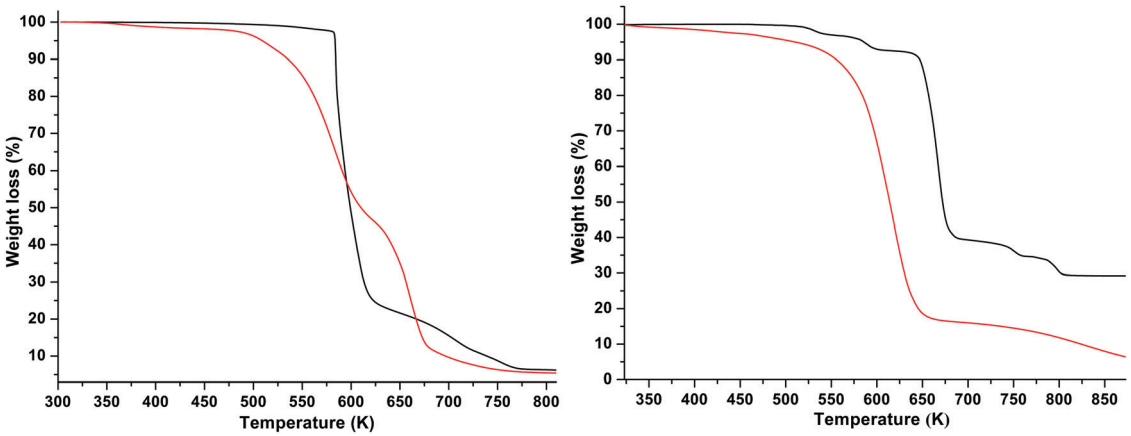

Fig. 7 TG curves of (left) $[P_{6,6,6,14}][BOB]$ prepared in this work (black) and previously reported $[P_{6,6,6,14}][BOB]$[9] before the heat treatment (red) and (right) Na[BOB] powder (black) and a liquid sample of $[P_{6,6,6,14}]Cl$ (red) at a heating rate of 10 K min^{-1}.

decomposition pathways of the starting compounds, products after Step I and final products (ILs). Percentage of the mass loss upon gradual heating (either at a "standard" heating rate of 10 K min^{-1} or at 1 K min^{-1}) of the samples was used as a descriptor of the thermal stability of ILs. TG curves of Na[BOB], $[P_{6,6,6,14}]Cl$, $[P_{6,6,6,14}][BOB]$ and $[P_{6,6,6,14}][BOB]$[9] (before the heat treatment) obtained at a heating rate of 10 K min^{-1} are shown in Fig. 7. In the dynamic TG analysis using a specifically ramped temperature program, the thermal stability of ILs is usually described by the T_{onset} point. By definition, T_{onset} is a value obtained from the intercept of two straight lines: the baseline of zero weight loss and the tangent of weight *vs.* temperature upon abrupt decomposition.[48] Note that T_{onset} is commonly used to compare the thermal stability of different ILs. Since the definition of T_{onset} is considerably affected by the initial inclination of the TGA curve (which is the case for $[P_{6,6,6,14}]Cl$ and $[P_{6,6,6,14}][BOB]$[9]), it gives an obvious overestimation of the true thermal stability, and actually creates more confusion than clarity. Hence, we decided to compare the data based on the sample weight loss of 2, 5 and 10%. This protocol has already been used by several research groups.[48,49]

$[P_{6,6,6,14}][BOB]$ was thermally stable up to 567 K with a weight loss of only 2 wt% (see Table 2). Note that $[P_{6,6,6,14}]Cl$ has shown a gradual weight loss already after 300 K with a maximum rate of the weight loss between 500 and 650 K (Fig. 7 right). The gradual weight loss of tetraalkylphosphonium chlorides is due to a stronger nucleophilicity of the chloride anion initiating de-alkylation reactions[50] and a partial vaporisation of the ILs in the form of coupled ion pairs with an increase in temperature.[51] It is important to note that $[P_{6,6,6,14}][BOB]$ exhibited a considerably better thermal stability compared with a sample of $[P_{6,6,6,14}][BOB]$[9] before the heat treatment (see Fig. 7 left and Table 2).

Table 2 Characteristic temperatures of the corresponding percent weight-losses from TGA curves of $[P_{6,6,6,14}][BOB]$ and $[P_{6,6,6,14}][BOB]$[9] before the heat treatment

Samples	$T_{2\%}$/K	$T_{5\%}$/K	$T_{10\%}$/K
$[P_{6,6,6,14}][BOB]$	567	583	584
$[P_{6,6,6,14}][BOB]$[9]	464	509	535

The results obtained from thermal analysis are dependent not only on the heating rate, but also on the sample weight, purge gas flow and type of pans used in the analysis.[52] In view of these factors, thermal stabilities of $[P_{6,6,6,14}][BOB]$ and $[P_{6,6,6,14}]Cl$ were additionally studied at a slower heating rate of 1 K min^{-1} and were compared with the results obtained at the heating rate of 10 K min^{-1} under otherwise the same conditions. The TG curves obtained at different heating rates are presented in Fig. S24 (ESI†), while the temperatures corresponding to the weight loss of 2, 5 and 10% are tabulated in Table S1 in the ESI.† The data reveal that the onset of the abrupt decomposition was decreased by *ca.* 35 and *ca.* 30 K for $[P_{6,6,6,14}][BOB]$ and $[P_{6,6,6,14}]Cl$, respectively, when the heating rate was changed from the traditionally used 10 K min^{-1} to 1 K min^{-1} (see Fig. S24 in the ESI†). One reason for this behaviour is the higher discrepancies between the true sample temperature and the programmed temperature at a higher heating rate.[52] However, this instrumental artefact cannot generate temperature differences of *ca.* 30–35 K. One can assume that these IL samples can thermally decompose over time even at constant temperature, particularly at elevated temperatures close to the point of the abrupt decomposition. Therefore, isothermal TG scans of $[P_{6,6,6,14}][BOB]$ and $[P_{6,6,6,14}]Cl$ were also performed, motivated by the fact that $[P_{6,6,6,14}]Cl$ starts to degrade at a significantly lower temperature than T_{onset} (Fig. S25 in the ESI†). Both isothermal scans and these at the heating rate of 1 K min^{-1} confirmed the higher thermal stability of the $[P_{6,6,6,14}][BOB]$ sample in comparison with both $[P_{6,6,6,14}]Cl$ and $[P_{6,6,6,14}][BOB]$[9] (before the heat treatment). In the latter sample, TAC starts to transform to $[BOB]^-$ at temperatures above 373 K releasing water molecules and then excess of water in the sample matrix may catalyse the hydrolysis and thermal degradation of other ions at considerably lower temperatures (by *ca.* 50–100 K, see Table 2). However, the sample of $[P_{6,6,6,14}][BOB]$[9] after the heat treatment at 413 K, *i.e.* at which TAC has already transformed into $[BOB]^-$ anions, also has a considerably lower thermal stability as compared to

$[P_{6,6,6,14}][BOB]$ (see Fig. S26 in the ESI†). We anticipate that the additional heat treatment of an impure $[P_{6,6,6,14}][BOB]$[9] at 413 K, may have led to the formation of other undesired impurities and then to a partial decomposition (dialkylation) and oxidation of $[P_{6,6,6,14}]^+$ cations at considerably lower temperatures (by almost 100 K). TGA curves of Na[BOB] revealed a weight loss of *ca.* 5 wt% at around 570 K and then an abrupt decomposition at *ca.* 650 K (*ca.* 50 wt% loss) and a final two-step weight loss (of *ca.* 5 wt% each around 750 and 800 K) with the formation of a residual white-grey inorganic material in the pan (*ca.* 31 wt%, 65 a.u., O_2BNa, see Fig. 7 right).

Differential scanning calorimetric (DSC) data were obtained by heating the samples from 173 to 373 K. Glass transition temperatures of $[P_{6,6,6,14}][BOB]$ and $[P_{6,6,6,14}][BOB]$[9] (before the heat treatment) were found to be 202 and 203 K, with maximum heat flows at 205 and 210 K for these two samples, respectively (Fig. S27 in the ESI†). Glass transition temperatures previously reported for $[P_{6,6,6,14}][BOB]$ from Merck was 201 K,[53] while for $[P_{6,6,6,14}][BOB]$[9] (before the heat treatment), it was 201.7 K.[9] A DSC thermogram of Na[BOB] revealed a melting, sublimation and decomposition endotherm at 638 K (ΔH_f = 432 J g^{-1}) (Fig. S28 in the ESI†).

Density and viscosity

Density of $[P_{6,6,6,14}][BOB]$ was compared with the previously reported data for $[P_{6,6,6,14}][BOB]$[9]. A significant decrease in density (by >3%) was observed in the whole temperature interval studied, from 293 to 353 K (Fig. 8). These differences are, apparently, due to the presence of aggregates of hydrophilic TACs in $[P_{6,6,6,14}][BOB]$[9] (before the heat treatment). The repulsive van der Waals forces between the hydrophilic groups of $[BOB]^-$ and TAC anions and hydrophobic alkyl groups of tetraalkylphosphonium cations cause a decrease in the density of this IL system. Densities of both $[P_{6,6,6,14}][BOB]$ and $[P_{6,6,6,14}][BOB]$[9] decrease linearly with temperature (see Fig. 8 and Table S2 in the ESI†) as for other orthoborate-based tetraalkylphosphonium ILs.[9]

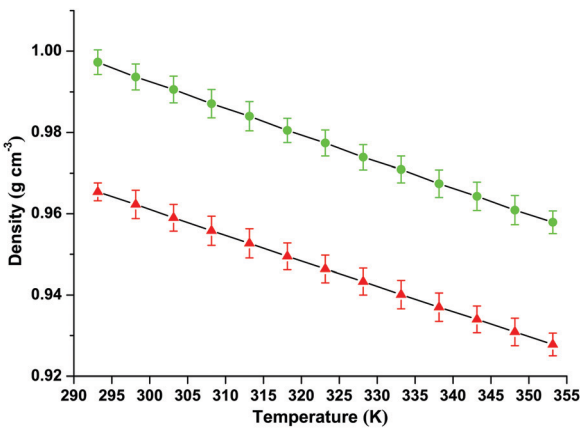

Fig. 8 Variations of densities of $[P_{6,6,6,14}][BOB]$ (circles) and $[P_{6,6,6,14}][BOB]$[9] before the heat treatment (triangles) as a function of temperature. Solid lines correspond to linear regressions, $\rho(T) = a + b{\cdot}T$ (for raw data and parameters a, b and R^2, see Table S2 in the ESI†).

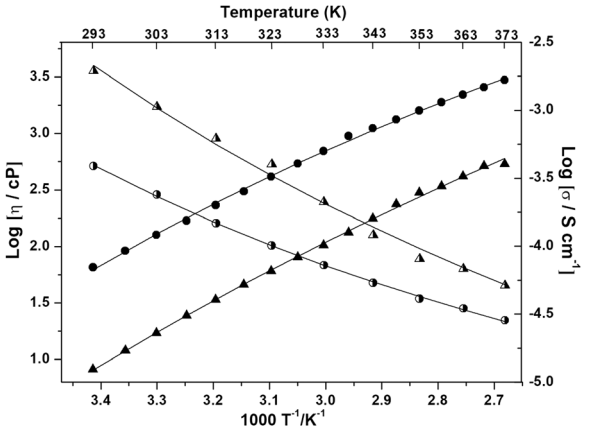

Fig. 9 Plots of dynamic viscosity and electrical conductivity of $[P_{6,6,6,14}][BOB]$ (circles) and $[P_{6,6,6,14}][BOB]$[9] before the heat treatment (triangles) as a function of the inverse temperature (1/*T*). Half-filled symbols correspond to viscosity, while solid symbols correspond to electrical conductivity. Corresponding fits using the VFT equations, eqn (1) and (2) for viscosity and electrical conductivity, respectively, are represented using solid lines (see Tables S3 and S5, ESI†). Error limits for data points are given in Tables S3 and S5 of the ESI.†

Dynamic viscosity values of $[P_{6,6,6,14}][BOB]$ and $[P_{6,6,6,14}][BOB]$[9] at different temperatures are tabulated in Table S3 in the ESI.† It can be seen that in the whole temperature range studied, the sample of $[P_{6,6,6,14}][BOB]$[9] (before the heat treatment) has a significantly higher viscosity compared to the $[P_{6,6,6,14}][BOB]$ sample prepared in this study. For example, at 293 K, the dynamic viscosities differ by seven-fold, *i.e.* 3.5792 and 0.513 Pa s for $[P_{6,6,6,14}][BOB]$[9] and $[P_{6,6,6,14}][BOB]$, respectively (see Table S3 in the ESI†). At 373 K, the dynamic viscosities of these two samples differ by *ca.* two-fold, *i.e.* 0.0451 and 0.0222 Pa s for $[P_{6,6,6,14}][BOB]$[9] and $[P_{6,6,6,14}][BOB]$, respectively (Table S3 in the ESI†). We suggest that the significantly higher dynamic viscosity of the $[P_{6,6,6,14}][BOB]$[9] sample is due to the extended hydrogen-bonded network built by TACs. Viscosity indexes for $[P_{6,6,6,14}][BOB]$ and $[P_{6,6,6,14}][BOB]$[9] are 171 and 97, respectively, as calculated from data in Tables S2–S4 of the ESI.†

To analyse viscosity–temperature dependence, $\log\eta$ is plotted against inverse temperature for investigated ILs as shown in Fig. 9 (*Y*-axis to the left). The experimental dynamic viscosity data were fitted using the Vogel–Fulcher–Tammann (VFT) equation[54,55]

$$\eta = \eta_0 \exp[B_\eta/(T - T_\eta^0)] \quad (1)$$

where η_0 (in mPa s), B_η (in K), and T_η^0 (in K) are fitting parameters. The best fit parameters for eqn (1) are tabulated in Table 3, and the solid lines in Fig. 9 represent the best fits from the VFT equation.

Ionic conductivity

The ionic conductivity of ILs is inversely proportional to their viscosities.[55] ILs are composed entirely of ions and can, therefore, be considered as concentrated electrolytes possessing mobile charge carriers. Electric conductivity of the investigated IL samples was measured in the temperature range from 293 to 373 K (Table S5 in the ESI†). Analogous to viscosity, the

Table 3 Correlation parameters for viscosity of $[P_{6,6,6,14}][BOB]$ and $[P_{6,6,6,14}][BOB]$[9] (before the heat treatment) obtained from the VFT equation (eqn (1)) in the range from 293 to 373 K

$\eta = \eta_0 \exp[B_\eta/(T - T_\eta^0)]$				
Samples	η_0/mPa s	B_η/K	T_η^0/K	R^2
$[P_{6,6,6,14}][BOB]$	0.480 ± 0.023	680 ± 1.4	196 ± 2	0.99834
$[P_{6,6,6,14}][BOB]$[9] (before the heat treatment)	0.100 ± 0.029	1200 ± 9	180 ± 2	0.98430

Table 4 Correlation parameters for the electrical conductivity of $[P_{6,6,6,14}][BOB]$ and $[P_{6,6,6,14}][BOB]$[9] (before the heat treatment) obtained from the VFT equation (eqn (2)) in the range from 293 to 373 K

$\sigma = \sigma_0 \exp[-B_\sigma/(T - T_\sigma^0)]$				
Samples	σ_0/S cm^{-1}	B_σ/K	T_σ^0/K	R^2
$[P_{6,6,6,14}][BOB]$	0.165 ± 0.093	880 ± 3.4	181 ± 2	0.99854
$[P_{6,6,6,14}][BOB]$[9] (before the heat treatment)	0.110 ± 0.086	1130 ± 4.2	169 ± 2	0.99768

temperature dependence of the ionic conductivity for each of the IL samples exhibits concave curves in Arrhenius plots and it can also be well described using the VFT equation.[54,55]

$$\sigma = \sigma_0 \exp[-B_\sigma/(T - T_\sigma^0)] \quad (2)$$

where σ_0 (in S cm^{-1}), B_σ (in K), and T_σ^0 (in K) are fitting parameters. The best fit parameters for eqn (2) are tabulated in Table 4, and the solid lines in Fig. 9 represent the best fit from the VFT equation. Interestingly, for conductivity data, T_σ^0 values were found to be rather close to T_g for $[P_{6,6,6,14}][BOB]$ (*ca.* 40 K deviation from T_g), which agrees well with other reports. The lower ionic conductivity of $[P_{6,6,6,14}][BOB]$[9] (before the heat treatment) as compared to that in $[P_{6,6,6,14}][BOB]$ is correlated with the viscosities of these samples: Conductivities of these samples differ by a factor of *ca.* 5.6 and 4.2 at 293 and 373 K, respectively (see Table S5 in the ESI†). In addition, in the sample of $[P_{6,6,6,14}][BOB]$[9] before the heat treatment, the TAC is prone to form clusters *via* hydrogen bonding networks. Therefore, mobilities of ions in this sample are lower, which in turn results in lower ionic conductivity. It is noteworthy that VFT fits of both viscosity and conductivity of $[P_{6,6,6,14}][BOB]$[9] (before the heat treatment) are worse than those of $[P_{6,6,6,14}][BOB]$ (see Fig. 9 and Tables 3 and 4). García *et al.* reported on the viscosity and conductivity of different orthoborate-based ILs with isobutyl(trihexyl)phosphonium cation.[56] Temperature dependence of viscosity and conductivity of isobutyl(trihexyl)phosphonium bis(oxalato)borate IL was measured and analysed using the VTF models. Though the tetraalkylphosphonium cation was different from that used in our study, we may anticipate the presence of TAC in their sample of isobutyl(trihexyl)phosphonium bis(oxalato)borate, because (i) viscosity of their sample is significantly high (by a factor of two at 313 K) compared with that of our "TAC-free" sample $[P_{6,6,6,14}][BOB]$; (ii) Na[BOB] was prepared with a 2 : 1 molar ratio of oxalic acid over boric acid (*i.e.* without any excess of oxalic acid over boric acid) and no further recrystallisation or washing of the crude sample with acetonitrile and ethanol were done before the metathesis reaction with isobutyl(trihexyl)phosphonium bromide; (iii) viscosity of another IL prepared by the same authors, namely isobutyl(trihexyl)phosphonium bis(malonato)borate, was found to be considerably lower in the whole temperature interval measured when compared to the viscosity of isobutyl(trihexyl)-phosphonium bis(oxalato)borate. The latter fact is in contradiction with obvious arguments that the additional two CH_2 groups in the bis(malonato)borate anion, in comparison to the bis(oxalato)borate anion, would lead to attractive van-der-Waals interactions with the alkyl groups of the cation and to a higher viscosity. This fact is confirmed by a range of studies on tetraalkylphosphonium orthoborate based ILs, including our own reports. However, no ^{11}B NMR spectra of isobutyl(trihexyl)phosphonium bis(oxalato)borate (and other) ILs are provided in ref. 56, which could reveal the presence of TAC and validate our hypothesis.

Conclusion

This work is a result of our quest for the causes of variation of viscosity and conductivity in different batches of $[P_{6,6,6,14}][BOB]$ (and [BOB]-based ILs with other cations) synthesised using either lithium or sodium salts of the bis(oxalato)borate anion as reported by us and by other research groups. It was found that the metastable transition anionic complexes (TACs) may be formed and passed into the final IL product. The physicochemical properties of $[P_{6,6,6,14}][BOB]$, synthesised with specific precautions on the sample purity (*i.e.* with only traces of the TACs), were investigated and compared to those of a previously reported sample of $[P_{6,6,6,14}][BOB]$[9] (before the heat treatment), which contained *ca.* 45 mol% of the TAC: a 1 : 1 complex of dihydroxy(oxalato)borate with oxalic acid, $[B(C_2O_4)(OH)_2 \cdot (HOOC–COOH)]^-$. In the latter sample, TACs are liable for strong hydrogen bonding forming clusters that, in turn, lead to a significant increase in viscosity, elevated water content (*ca.* 1.2 wt% determined by the indirect coulometric Karl Fischer titration) that is not removable even after prolonged drying in a vacuum oven, a lower density, a lower thermal stability and a considerable decrease in conductivity. Therefore, data obtained in this work for $[P_{6,6,6,14}][BOB]$ can now be used with a higher degree of confidence by the scientific community. In addition, any

significant deviation from the data reported here, in particular a higher-than-expected viscosity and a low-than-expected conductivity of $[P_{6,6,6,14}][BOB]$, would indicate the possible presence of TACs as impurities in the samples of this IL. It was also found that TACs transform into $[BOB]^-$ anions upon heating at 413 K for *ca.* one hour. However, it is important to note that even after the transformation of TACs into $[BOB]^-$ anions followed by the evaporation of water formed during this reaction, the sample does not reach the same level of purity as that of $[P_{6,6,6,14}][BOB]$, when thoroughly purified Na[BOB] was used in the metathesis reaction under mild conditions (at 323–333 K). Therefore, an additional heating of an impure $[P_{6,6,6,14}][BOB]$ may only improve its purity to a certain degree and only with respect to specific boron-containing impurities, such as TACs discussed here. However, any additional post-treatment of an impure $[P_{6,6,6,14}][BOB]$ at elevated temperatures may also lead to the formation of other undesired impurities due to the partial decomposition and oxidation of the $[P_{6,6,6,14}]^+$ cation. Based on the above findings for the specific case of the room-temperature ionic liquid $[P_{6,6,6,14}][BOB]$, this work is a message to all reviewers of reports on newly designed and prepared ILs, to more thoroughly check and request for (if missing) the elemental analysis, water content and NMR data of the final IL products, which could highlight the actual presence of sub-percent amounts of impurities, such as TACs in ILs. As demonstrated in this work, some of the TACs trapped in ILs may severely alter the physico-chemical properties of ILs, which, in turn, may lead to irreproducible results and uncontrolled performance in some applications of these ILs.

Experimental

Chemicals

Boric acid (99.999%) and anhydrous oxalic acid (99.999%) were purchased from Aldrich Chemicals, while sodium carbonate (99.999%) was purchased from Merck. Lithium carbonate (99.9%), acetonitrile, ethanol (97.5%) and dichloromethane (DCM) were purchased from Sigma-Aldrich and used as supplied. Trihexyl(tetradecyl)phosphonium chloride (98%) was purchased from Solvionic. Milli-Q water (electric conductivity less than 0.1 μS cm^{-1}) was used in the synthesis and all experiments. A sample of previously reported $[P_{6,6,6,14}][BOB]$ in ref. 9 was also characterised and used as a reference sample, denoted here as $[P_{6,6,6,14}][BOB]^9$ for the comparative studies of physico-chemical properties of these IL samples.

Synthesis of lithium bis(oxalato)borate, Li[BOB]

Oxalic acid (1.8 g, 20 mmol) and boric acid (0.618 g, 10 mmol) were separately dissolved in water and then mixed together under constant stirring. Li_2CO_3 (0.369 g, 5 mmol) was added slowly to the mixture with vigorous stirring. The solution was heated up to 333 K and stirred for two hours. The reaction mixture was then cooled down to room temperature. Water was removed using a rotatory evaporator. The crude product was then washed in acetonitrile and the final product was isolated as a white precipitate by vacuum filtration (yield was 85%).

Synthesis of sodium bis(oxalato)borate, Na[BOB]

Oxalic acid (1.8 g, 20 mmol) and boric acid (0.618 g, 10 mmol) were separately dissolved in water and then mixed together under constant stirring. Na_2CO_3 (0.53 g, 5 mmol) was slowly added to the mixture with vigorous stirring. The turbid solution was heated in an oil bath at 393 K until a dry white powder was obtained. The crude product was dispersed in hot acetonitrile at 333 K and stirred for one more hour. Then a white powder was isolated using vacuum filtration. The product was further washed with cold ethanol and the powder was dried in an oven at 333 K for 12 hours.

Additional samples were also prepared using different molar ratios of reagents (boric acid : oxalic acid : sodium carbonate; 1 : 1 : 0.5, 1 : 1.5 : 0.5, 1 : 2 : 0.5, 1 : 2.1 : 0.5, 1 : 2.5 : 0.5 and 1 : 3 : 0.5) as per the above-mentioned procedure.

Synthesis of trihexyl(tetradecyl)phosphonium bis(oxalato)borate, $[P_{6,6,6,14}][BOB]$

The obtained Na[BOB] powder (2.10 g, *ca.* 0.010 mol) was mixed with (5.19 g, 0.01 mol) trihexyl(tetradecyl)phosphonium chloride, *i.e.* at an equimolar ratio in 30 mL of dichloromethane. The reaction mixture was stirred for 20 hours at room temperature and then water was added under continuous stirring. Consequently, the organic layer was isolated and additionally washed with 100 mL of water to remove traces of Na^+ and Cl^- ions. Dichloromethane was rotary evaporated at reduced pressure and the product was dried in a vacuum oven at 333 K for 2 days. A colourless liquid, $[P_{6,6,6,14}][BOB]$ was obtained with a yield of $>95\%$.

NMR characterisation

Solid-state ^{11}B magic-angle-spinning (MAS) NMR spectra for all the prepared sodium and lithium salt materials (before and after washing) were obtained at 115.47 MHz using a Chemagnetics InfinityPlus CMX-360 (B_0 = 8.46 T) spectrometer with a 3.2 mm MAS probe or/and at 128.40 MHz using an Avance III NMR spectrometer (Bruker BioSpin AG, Fällanden, Switzerland) with Aeon 9.4 T zero-helium boil-off superconducting magnet using a Varian 4.0 mm MAS probe. The samples were packed as fine ground powder in standard 3.2 mm or/and 4.0 mm ZrO_2 rotors. Single-pulse direct-excitation ^{11}B MAS NMR experiments were employed with a spinning frequency manually set (±5 Hz) at 8 kHz (for 4 mm rotors) and 12 kHz (for 3.2 mm rotors) to minimise the integral intensity of the spinning sidebands. However, when the relative quantities of different boron containing species were analysed, integrals of spinning sidebands were also taken into account in the analysis (see Fig. S4 and S6 in the ESI†). All spectra were externally referenced using a liquid sample of borontrifluoride diethyletherate ($BF_3{\cdot}Et_2O$) filled in a small glass capillary and placed in empty 3.2 mm zirconia rotors. In CMX-360, for ^{11}B, the π/2-pulse was set to 2.5 μs, calibrated using a liquid reference sample of $BF_3{\cdot}Et_2O$. Then, for solid-state NMR measurements, a "quadrupolar" excitation π/4-pulse of 1.25 μs was used in the single-pulse experiments with a recycling delay of 2 s (^{11}B, $I = 3/2$, therefore, nutation frequency was set to $\omega_{nut} = (I + 1/2)\omega_1 = 2\omega_1$). For Li[BOB] crude samples, the ^{11}B MAS NMR

spectra were obtained using a Bruker-400 at 8 kHz spinning, with the excitation π/8-pulse (22.5°) of 1.2 μs in a 4 mm MAS probe, and recycle delay of 10 s to avoid the differential signal saturation for the main compound (Li[BOB]) and boron containing impurities (the number of signal transients was from 300 to 1464 for different samples). The relative integral intensity of resonance lines corresponding to different boron-based species present in the samples was determined by deconvolution of the ^{11}B NMR spectra using a spectrometer built-in "Spinsight" (on CMX-360) or "TopSpin 3.5" (on Bruker-400) software. The resonance lines were deconvoluted with the best fit using 50 : 50% Lorenzian and Gaussian. The deconvolution errors (integrals of resonance lines) were in the range of ±0.5–1.5% for all ^{11}B NMR spectra. The appropriate number of signal transients were acquired to obtain a signal-to-noise ratio (S/N) > 100 for both ^{11}B MAS and ^{31}P static NMR spectra.

Solution ^{1}H, ^{13}C, ^{11}B and ^{31}P NMR spectra of IL samples (in $CDCl_3$) were performed using a Bruker Avance III NMR spectrometer (Bruker BioSpin AG, Fällanden, Switzerland) with an Aeon 9.4 T zero-helium boil-off superconducting magnet and 10 mm and 5 mm probes for liquids. Working frequencies were 400.27 MHz for ^{1}H, 100.64 for ^{13}C, 128.4 MHz for ^{11}B and 162.000 MHz for ^{31}P. Proton decoupling pulse sequence WALTZ-16 was used for ^{13}C NMR. π/2 pulse durations were 7 μs, 15 μs, 9 μs and 10 μs for ^{1}H, ^{13}C, ^{11}B and ^{31}P, respectively. Teramethylsilane (TMS) was used as the internal reference for ^{1}H and ^{13}C, while boron trifluoride diethyl etherate ($BF_3{\cdot}OEt_2$) and 85% H_3PO_4 (in a separate 5 mm tube inserted into a 10 mm sample tube) were used as the external references for ^{11}B and ^{31}P, respectively.

Powder X-ray diffraction (PXRD)

PXRD patterns of the samples were collected using an Empyrean X-ray diffractometer (PANalytical, The Netherlands) equipped with a PIXel3D detector and a monochromatic Cu Kα1 radiation X-ray tube (λ = 1.54056 Å). The tube voltage and amperage were set at 45 kV and 40 mA, respectively. Samples were filled into a metal holder and flattened. Instrument calibration was performed using a silicon reference standard. Each sample was scanned at a 2θ range from 5 to 40°, increasing at a step size of 0.02°. The data were processed using HighScore Plus software (PANalytical, The Netherlands).

Differential scanning calorimetry (DSC)

Thermal analyses of the samples were performed using a DSC 6000 PerkinElmer equipped with an external Portable Cooling Device (PCD). Each sample (1–2 mg) was accurately weighted and placed into an aluminium DSC pan. The pan was crimped and the contents precooled under a nitrogen atmosphere using PCD. The samples were heated from 173 to 373 K at a heating rate of 10 K min^{-1} under a nitrogen gas flow rate of 20.0 mL min^{-1}. Indium was used as the calibration standard. The glass transition temperature was determined using Pyris software. The data for each sample were collected in duplicate.

Thermogravimetric analysis (TGA)

Thermogravimetric analysis (TGA) was performed using an 8000 PerkinElmer thermogravimetric analyser with heating rates of 10 and 1 K min^{-1}. Test samples (2–3 mg) were placed in a ceramic crucible and then inserted into the TG furnace. The measurements were performed with a nitrogen gas flow rate of 20.0 mL min^{-1}. The temperature corresponding to the loss of 2, 5 and 10% of weight was determined using the Pyris software. The data for each sample were collected in duplicate.

Density and viscosity

An Anton Paar DMA 4100M density meter was used to measure the density of $[P_{6,6,6,14}][BOB]$ and $[P_{6,6,6,14}][BOB]$[9] (before the heat treatment) in the temperature range from 293 to 353 K. The density meter was calibrated using air media and Millipore water at 293 K. The data for each sample were collected in duplicate.

Dynamic viscosity was measured using a TA Instruments HR3 rheometer (parallel plate configuration with a diameter of 20 mm) in the temperature range from 293 to 373 K in steps of 10 K. Prior to each measurement, the sample temperature was stabilised for 20 min. The measurement time at each temperature step was 120 s. The shear rate was kept constant at 10 s^{-1} to avoid any shear thinning effects. All measurements were carried out under a dry air atmosphere in an environmental chamber. The rheometer was calibrated by measuring the viscosity of a calibration oil in the same temperature range.

Karl Fischer titration

The water content of the ILs was measured by coulometric Karl Fischer titration with diaphragm (Metrohm 831 KF). We found that the water content of the prepared ILs was dependent on the amount of IL added. Hence, the water content of these ILs was determined by an indirect method (oven method) using coulometric Karl Fischer titration. In this method, the sample was heated in an oven to approximately 403 K (ILs do not decompose while releasing water vapour). The released water vapour was transferred by flow of a dry carrier gas to the titration cell, where water content was determined by coulometric Karl Fischer titration.

Ionic conductivity

The electrical conductivity of the IL samples was measured by employing a Metrohm Autolab PGSTAT302N electrochemical workstation equipped with a FRA32M module for impedance measurements, all controlled by the Nova 2.02 software. Measurements were carried out with frequencies ranging from 1 MHz down to 1 Hz with an excitation amplitude of 10 mV_{rms} AC. All measurements were conducted within a temperature range from 293 to 373 K. Thermal equilibrium was achieved for 20 min prior to each measurement. The sample cell volume was 70 μL. The two-electrode system consisted of a Pt-wire (diameter 0.25 mm) as the working electrode and the sample cell container made from platinum as the counter electrode. The electrodes were polished with a Kemet diamond paste 0.25 μm prior to each measurement. KCl standard solution (from Metrohm) with an electric conductivity of 100 μS cm^{-1} was employed to determine

the cell conductivity constant (K_{cell} = 17.511 cm^{-1}). The characteristic conductivity at each temperature was determined by fitting measured resistivity of the liquid to an equivalent electric circuit.

Author contributions

Following the CRediT (the Contributor Roles Taxonomy from CASRAI) standardised contribution descriptions, the co-authors roles were identified, discussed and approved by all contributors as: (i) conceptualisation (MRS, SG, ONA); (ii) formal analysis (MRS, PR, ONA); (iii) funding acquisition (SG, ONA, FUS); (iv) investigation (MRS, PR, FUS, ONA); (v) methodology (MRS, ONA, SG); (vi) project administration (SG, ONA); (vii) resources (MRS, SG, PR, FUS, ONA); (vii) supervision (SG, ONA); (viii) validation (SG, ONA); (ix) visualisation (MRS, PR, ONA); (x) writing – original draft (MRS, ONA, PR); and (xi) writing – review & editing (ONA, MRS, SG, PR, FUS).

Conflicts of interest

ONA, SG and FUS are holders of patents: SE 535676 and JP 5920900.

Acknowledgements

The Knut and Alice Wallenberg Foundation (project number KAW 2012.0078), the Swedish Research Council (project numbers 2013-5171 (ONA), 2014-4694 (SG) and 2018-05017 (SG)) and the Swedish Foundation for Strategic Research (Grant EM16-0013) are gratefully acknowledged for their financial support. We also thank the Foundation in memory of J. C. and Seth M. Kempe (project numbers JCK-1306 and JCK-1433) and the laboratory fund at LTU for providing grants, from which a Bruker Aeon/Avance III NMR spectrometer at LTU has been purchased. We thank Dr Andrei Filippov for helping with the VFT analysis of dynamic viscosity and electrical conductivity data using Origin software.

References

1 N. V. Plechkova and K. R. Seddon, Applications of ionic liquids in the chemical industry, *Chem. Soc. Rev.*, 2008, **37**, 123–150.
2 X. Wang, C. André Ohlin, Q. Lu, Z. Fei, J. Hu and P. J. Dyson, Cytotoxicity of ionic liquids and precursor compounds towards human cell line HeLa, *Green Chem.*, 2007, **9**, 1191–1197.
3 S. Stolte, J. Arning, U. Bottin-Weber, M. Matzke, F. Stock, K. Thiele, M. Uerdingen, U. Welz-Biermann, B. Jastorff and J. Ranke, Anion effects on the cytotoxicity of ionic liquids, *Green Chem.*, 2006, **7**, 621–629.
4 M. Smiglak, A. Metlen and R. D. Rogers, The second evolution of ionic liquids: from solvents and separations to advanced materials-energetic examples from the ionic liquid cookbook, *Acc. Chem. Res.*, 2007, **40**, 1182–1192.
5 S. V. Dzyuba and R. A. Bartsch, Recent advances in applications of room-temperature ionic liquid/supercritical CO_2 systems, *Angew. Chem., Int. Ed.*, 2003, **42**, 148–150.
6 S. M. Zakeeruddin and M. Graetzel, Solvent-free ionic liquid electrolytes for mesoscopic dye-sensitized solar cells, *Adv. Funct. Mater.*, 2009, **19**, 2187–2202.
7 F. Zhou, Y. Liang and W. Liu, Ionic liquid lubricants: designed chemistry for engineering applications, *Chem. Soc. Rev.*, 2009, **38**, 2590–2599.
8 I. Minami, Ionic liquids in tribology, *Molecules*, 2009, **14**, 2286–2305.
9 F. U. Shah, S. Glavatskih, D. R. MacFarlane, A. Somers, M. Forsyth and O. N. Antzutkin, Novel halogen-free chelated orthoborate-phosphonium ionic liquids: Synthesis and tribophysical properties, *Phys. Chem. Chem. Phys.*, 2011, **13**, 12865–12873.
10 F. U. Shah, S. Glavatskih and O. N. Antzutkin, Boron in tribology: From borates to ionic liquids, *Tribol. Lett.*, 2013, **51**, 281–301.
11 A. E. Somers, P. C. Howlett, D. R. MacFarlane and M. Forsyth, A review of ionic liquid lubricants, *Lubricants*, 2013, **1**, 3–21.
12 R. Gusain, R. Singh, K. Sivakumar and O. P. Khatri, Halogen-free imidazolium/ammonium bis(salicylato)borate ionic liquids as high-performance lubricant additives, *RSC Adv.*, 2014, **4**, 1293–1301.
13 R. Gusain and O. P. Khatri, Halogen-free ionic liquids: Effect of chelated orthoborate anion structure on their lubrication properties, *RSC Adv.*, 2015, **5**, 25287–25294.
14 X. Fan and L. Wang, Highly conductive ionic liquids toward high-performance space-lubricating greases, *ACS Appl. Mater. Interfaces*, 2014, **6**, 14660–14671.
15 P. Rohlmann, B. Munavirov, I. Furó, O. N. Antzutkin, M. Rutland and S. Glavatskih, Non-halogenated ionic liquid dramatically enhances tribological performance of biodegradable oils, *Front. Chem.*, 2019, **7**, 98.
16 H. Li, A. E. Somers, P. C. Howlett, M. W. Rutland, M. Forsyth and R. Atkin, Addition of low concentrations of an ionic liquid to a combined nano- and microtribology investigation, *Phys. Chem. Chem. Phys.*, 2016, **18**, 6541–6547.
17 B. A. Rosen, A. Salehi-Khojin, M. R. Thorson, W. Zhu, D. T. Whipple, P. J. A. Kenis and R. I. Masel, Ionic liquid-mediated selective conversion of CO_2 to CO at low overpotentials, *Science*, 2011, **334**, 643–644.
18 Y. Zhang, H. Gao, Y. H. Joo and J. M. Shreeve, Ionic liquids as hypergolic fuels, *Angew. Chem., Int. Ed.*, 2011, **50**, 9554–9562.
19 T. Ogoshi, T. Onodera, T. Yamagishi, Y. Nakamoto, A. Kagata, N. Matsumi and K. Aoi, Transparent ionic liquid-phenol resin hybrids with high ionic conductivity, *Polym. J.*, 2011, **43**, 421–424.
20 M. Matsumoto, Y. Saito, C. Park, T. Fukushima and T. Aida, Ultrahigh-throughput exfoliation of graphite into pristine 'single-layer' graphene using microwaves and molecularly engineered ionic liquids, *Nat. Chem.*, 2015, **7**, 730–736.
21 M. R. Shimpi, S. P. Velaga, F. U. Shah and O. N. Antzutkin, Pharmaceutical crystal engineering using ionic liquid anion-solute interactions, *Cryst. Growth Des.*, 2017, **17**, 1729–1734.

22 J. A. Widegren, A. Laesecke and J. W. Magee, The effect of dissolved water on the viscosities of hydrophobic room-temperature ionic liquids, *Chem. Commun.*, 2005, 1610–1612.
23 J.-M. Andanson, X. Meng, M. Traïkia and P. Husson, Quantification of the impact of water as an impurity on standard physico-chemical properties of ionic liquids, *J. Chem. Thermodyn.*, 2016, **94**, 169–176.
24 J. A. Widegren, E. M. Saurer, K. N. Marsh and J. W. Magee, Electrolytic conductivity of four imidazolium-based room-temperature ionic liquids and the effect of a water impurity, *J. Chem. Thermodyn.*, 2005, **37**, 569–575.
25 R. Jarosova and G. M. Swain, Rapid preparation of room temperature ionic liquids with low water content as characterized with a t_a-C:N electrode, *J. Electrochem. Soc.*, 2015, **162**, H507–H511.
26 C. Villagran, M. Deetlefs, W. R. Pitner and C. Hardacre, Quantification of halide in ionic liquids using ion chromatography, *Anal. Chem.*, 2004, **76**, 2118–2123.
27 T. van der Hoogerstraete, S. Jamar, S. Wellens and K. Binnemans, Determination of halide impurities in ionic liquids by total reflection X-ray fluorescence spectrometry, *Anal. Chem.*, 2014, **86**, 3931–3938.
28 K. McCamley, N. A. Warner, M. M. Lamoureux, P. J. Scammells and R. D. Singer, Quantification of chloride ion impurities in ionic liquids using ICP-MS analysis, *Green Chem.*, 2004, **6**, 341–344.
29 A. Stark, P. Behrend, O. Braun, A. Mueller, J. Ranke, B. Ondruschka and B. Jastorff, Purity specification methods for ionic liquids, *Green Chem.*, 2008, **10**, 1152–1161.
30 P. A. Z. Suarez, S. Einloft, J. E. L. Dullius, R. F. de Souza and J. Dupont, Synthesis and physical–chemical properties of ionic liquids based on 1-*n*-butyl-3-methylimidazolium cation, *J. Chim. Phys. Phys.-Chim. Biol.*, 1998, **95**, 1626–1639.
31 L. C. Branco, J. N. Rosa, J. J. M. Ramos and C. A. M. Afonso, Preparation and characterization of new room temperature ionic liquids, *Chem. – Eur. J.*, 2002, **8**, 3671–3677.
32 W. Xu, L. Wang, R. A. Nieman and C. A. Angell, Ionic liquids of chelated orthoborates as model ionic glassformers, *J. Phys. Chem. B*, 2003, **107**, 11749–11756.
33 P. Y. Zavalij, S. Yang and M. S. Whittingham, Structural chemistry of new lithium bis(oxalato)borate solvates, *Acta Crystallogr., Sect. B: Struct. Sci.*, 2004, **60**, 716–724.
34 I. A. Shkrob, Y. Zhu, T. W. Marin and D. P. Abraham, Mechanistic insights into the protective action of bis(oxalato)borate and difluoro(oxalato)borate anions in Li-ion batteries, *J. Phys. Chem. C*, 2013, **117**, 23750–23756.
35 F. Lian, Y. Li, Y. He, H. Guan, K. Yan, W. Qiu, K.-C. Chou, P. Axmann and M. Wohlfahrt-Mehrens, Preparation of LiBOB *via* rheological phase method and its application to mitigate voltage fade of $Li_{1.16}[Mn_{0.75}Ni_{0.25}]_{0.84}O_2$ cathode, *RSC Adv.*, 2015, **5**, 86763–86770.
36 G. Hernández, A. J. Naylor, Y.-C. Chien, D. Brandell, J. Mindemark and K. Edström, Elimination of fluorination: the influence of fluorine-free electrolytes on the performance of $LiNi_{1/3}Mn_{1/3}Co_{1/3}O_2$/silicon-graphite Li-ion battery cells, *ACS Sustainable Chem. Eng.*, 2020, **8**, 10041–10052.
37 C. Ge, L. Wang, L. Xue, Z. Wu, H. Li, Z. Gong and X. Zhang, Synthesis of novel organic-ligand-doped sodium bis(oxalato)-borate complexes with tailored thermal stability and enhanced ion conductivity for sodium ion batteries, *J. Power Sources*, 2014, **248**, 77–82.
38 R. Mogensen, S. Colbin, A. Sreekumar Menon, E. Björklund and R. Younesi, Sodium bis(oxalato)borate in trimethyl phosphate: a fire-extinguishing, fluorine-free, and low-cost electrolyte for full-cell sodium-ion batteries, *ACS Appl. Energy Mater.*, 2020, **3**, 4974–4982.
39 F. Larsson, P. Andersson, P. Blomqvist and B.-E. Mellander, Toxic fluoride gas emission from lithium-ion battery fires, *Sci. Rep.*, 2017, **7**, 10018.
40 P. Schmitz, R. Jakelski, K. Jalkanen, M. Winter and P. Bieker, Synthesis of high-purity imidazolium tetrafluoroborates and bis(oxalato)borates, *Chem. – Eur. J.*, 2017, **23**, 2261–2264.
41 P. Rohlmann, S. Watanabe, M. Shimpi, J. Leckner, J. Harper, M. Rutland and S. Glavatskih, Boundary lubricity of phosphonium bisoxalatoborate ionic liquids, 2020, submitted.
42 L. Yang, M. M. Furczon, A. Xiao, B. L. Lucht, Z. Zhang and D. P. Abraham, Effect of impurities and moisture on lithium bis(oxalato)borate (LiBOB) electrolyte performance in lithium-ion cells, *J. Power Sources*, 2010, **195**, 1698–1705.
43 S. I. Lall-Ramnarine, A. Castano, G. Subramaniam, M. F. Thomas and J. F. Wishart, Synthesis, characterization and radiolytic properties of bis(oxalato)borate containing ionic liquids, *Radiat. Phys. Chem.*, 2009, **78**, 1120–1125.
44 J. M. Carr, P. J. Duggan, D. G. Humphrey, E. M. Tyndall and J. M. White, Quaternary ammonium spiroborate esters and mixed anhydrides derived from aliphatic α-hydroxy acids and diacids and their wood protection properties, *Aust. J. Chem.*, 2011, **64**, 1417–1424.
45 S. Kroeker and J. F. Stebbins, Three-coordinated boron-11 chemical shifts in borates, *Inorg. Chem.*, 2001, **40**, 6239–6246.
46 J. M. Carr, P. J. Duggan, D. G. Humphrey, J. A. Platts and E. M. Tyndall, Quaternary ammonium arylspiroborate esters as organo-soluble, environmentally benign wood protectants, *Aust. J. Chem.*, 2005, **58**, 901–911.
47 M. R. Shimpi, N. Seethalekshmi and V. R. Pedireddi, Supramolecular architecture in some 4-halophenylboronic acids, *Cryst. Growth Des.*, 2007, **7**, 1958–1963.
48 C. Maton, N. de Vos and C. V. Stevens, Ionic liquid thermal stabilities: decomposition mechanisms and analysis tools, *Chem. Soc. Rev.*, 2013, **42**, 5963–5977.
49 K. Noack, P. S. Schulz, N. Paape, J. Kiefer, P. Wasserscheid and A. Leipertz, The role of the C_2 position in interionic interactions of imidazolium based ionic liquids: a vibrational and NMR spectroscopic study, *Phys. Chem. Chem. Phys.*, 2010, **12**, 14153–14161.
50 H. Shirota, T. Mandai, H. Fukazawa and T. Kato, Comparison between dicationic and monocationic ionic liquids: Liquid density, thermal properties, surface tension, and shear viscosity, *J. Chem. Eng. Data*, 2011, **56**, 2453–2459.
51 M. Golets, M. R. Shimpi, Y.-L. Wang, O. N. Antzutkin, S. Glavatskih and A. Laaksonen, Understanding the thermal decomposition mechanism of a halogen-free chelated orthoborate-based ionic

liquid: a combined computational and experimental study, *Phys. Chem. Chem. Phys.*, 2016, **18**, 22458–22466.

52 M. J. Earle, J. M. S. S. Esperanca, M. A. Gilea, J. N. Canongia Lopes, L. P. N. Rebelo, J. W. Magee, K. R. Seddon and J. A. Widegren, The distillation and volatility of ionic liquids, *Nature*, 2006, **439**, 831–834.

53 M. Villanueva, A. Coronas, J. Garcia and J. Salgado, Thermal stability of ionic liquids for their application as new absorbents, *Ind. Eng. Chem. Res.*, 2013, **52**, 15718–15727.

54 L. Sun, O. Morales-Collazo, H. Xia and J. F. Brennecke, Physicochemical properties and structures of room-temperature ionic liquids. 3. Variation of cationic structures, *J. Phys. Chem. B*, 2016, **120**, 5767–5776.

55 F. U. Shah, O. I. Gnezdilov and A. Filippov, Ion dynamics in halogen-free phosphonium bis(salicylato)borate ionic liquid electrolytes for lithium-ion batteries, *Phys. Chem. Chem. Phys.*, 2017, **19**, 16721–16730.

56 A. García, L. C. Torres-Gonzáles, K. P. Padmasree, M. G. Benavidez-Garcia and E. M. Sánchez, Conductivity and viscosity properties of associated ionic liquids phosphonium orthoborates, *J. Mol. Liq.*, 2013, **178**, 57–62.